VOL. 21, NO. 7, APRIL 2026 ISSN 1819-6608
ARPN Journal of Engineering and Applied Sciences

www.arpnjournals.com

LOW-CARBON BINDER DEVELOPMENT USING SILICA FUME, GGBS AND COAL-WASHERY REJECTS AND ELEVATION OF MECHANICAL PERFORMANCE WITH ENVIRONMENTAL SIGNIFICANCE

Shashidhar Reddy G. and Ramesh B.
Department of Civil Engineering, Saveetha School of Engineering, SIMATS, Chennai, Tamil Nadu, India
E-Mail: shashidharreddygujja@gmail.com

ABSTRACT

This study examines the chemical characteristics, microstructural behaviour and strength evolution of a low-carbon blended binder incorporating silica fume (15%), ground granulated blast-furnace slag (20%), coal-washery rejects (15%) and ordinary Portland cement (50%). Coal-washery rejects were processed to a particle size below 75 µm and utilized as a supplementary component within the binder system. Elemental characterization using SEM-EDS confirmed the presence of oxygen (44.6%), silicon (13.3%), calcium (10.4%), carbon (8.9%), iron (6.0%), aluminum (5.1%), potassium (3.4%), phosphorus (3.3%), magnesium (1.7%), titanium (0.6%) and sodium (0.6%), indicating a mineralogical composition compatible with cementitious reactions. Microstructural assessment revealed the development of a dense hydration matrix dominated by calcium-silicate-hydrate (C-S-H) gel and uniformly distributed reaction products. SEM-EDS mapping demonstrated effective interaction among silica fume, GGBS, and coal-washery rejects, with silica fume enhancing secondary C-S-H formation and GGBS contributing to sustained hydration and matrix densification. Progressive refinement of gel phases and Si-Ca co-located regions was observed with curing, supporting continuous strength development. Compressive strength increased steadily from 24.8 MPa at 3 days to 34.2 MPa at 7 days, 48.9 MPa at 28 days, and 58.3 MPa at 90 days, reflecting effective hydration and microstructural evolution. Thermal and phase analyses further confirmed partial consumption of portlandite and increased amorphous gel formation, consistent with strong pozzolanic and latent hydraulic activity. From an environmental perspective, replacing 50% of ordinary Portland cement with industrial byproducts substantially reduces clinker demand and associated CO_2 emissions while enabling beneficial utilization of coal-washery waste. The results demonstrate that coal-washery rejects can be effectively integrated into silica fume and GGBS-based blended binders, providing a technically robust and environmentally sustainable pathway for low-carbon cementitious material development.

Keywords: silica fume, GGBS, CWR, SEM-EDS analysis, low-carbon binders, hydration chemistry, and sustainable cementitious materials.

Manuscript Received 9 March 2026; Revised 5 April 2026; Published 10 June 2026

INTRODUCTION

The growing demand for sustainable construction materials has intensified the search for low-carbon alternatives to ordinary Portland cement (OPC) [21]. Cement production is responsible for nearly 7-8% of global CO_2 emissions due to the energy-intensive clinker manufacturing process [8]. As urbanization accelerates, the pressure to reduce environmental impacts while maintaining structural performance has driven researchers to investigate supplementary cementitious materials (SCMs) that can partially replace OPC [14]. Among various SCMs, silica fume (SF) and ground granulated blast-furnace slag (GGBS) have received considerable attention for their ability to enhance hydration, refine microstructure, and improve the mechanical performance of blended binders [35]. Their pozzolanic and latent hydraulic reactions promote the formation of additional calcium-silicate-hydrate (C-S-H), leading to reduced porosity and improved long-term durability [28-35]. Parallel to the use of industrial byproducts like SF and GGBS, the valorization of coal-washery rejects (CWR) has gained importance, particularly in coal-producing regions. CWR is generated during the beneficiation and washing of raw coal, producing large quantities of solid waste that often accumulate in heaps, contributing to land degradation, leachate issues, and environmental hazards. In India, the Singareni Collieries Company Limited (SCCL), located in Bhadradri Kothagudem District, Telangana, produces substantial volumes of washery rejects. These materials typically contain oxides of silicon, aluminum, iron, and calcium, offering potential for use as low-reactivity mineral additions in cementitious systems. Reusing such waste in construction materials not only reduces environmental burdens but also aligns with circular-economy principles by transforming underutilized byproducts into functional components. The integration of CWR with high SCM blended binders can be particularly beneficial when combined with SF and GGBS, as the combined system leverages multiple reaction mechanisms. Silica fume contributes extremely fine particles and high amorphous silica content, accelerating early pozzolanic reactions and enhancing packing density. GGBS participates predominantly in long-term hydration through slag activation in alkaline environments, improving strength evolution beyond standard curing periods. When CWR is processed to fine particle sizes, it can act as a

microfiller, improve matrix homogeneity and, depending on its mineralogical composition, contribute to secondary hydration reactions. Such synergistic effects provide pathways for developing low-carbon binders with reduced OPC content without compromising strength and microstructural performance.

However, the effective incorporation of CWR into cementitious materials depends on carefully evaluating its chemical characteristics [14, 18, 23, 24, 32]. Variability in coal sources, beneficiation conditions, and mineral constituents may influence its compatibility with blended binders [45, 47, 50-58]. Therefore, detailed elemental characterization is essential before using CWR as a partial replacement material. In this context, the present study utilizes CWR collected from SCCL, processed to <75 μm, and incorporated at a 15% replacement level within a binder system also containing silica fume, GGBS, and 50% OPC [4,36]. Understanding how this combination behaves in terms of hydration, mechanical response and microstructural development is critical for assessing its viability in sustainable construction applications [9, 25-29]. This research aims to advance scientific knowledge related to low-carbon binders formulated with multiple SCMs and coal-derived industrial waste [22]. The study integrates material characterization, mix development, mechanical testing, and microstructural evaluation to establish a comprehensive understanding of how SCCL-based CWR interacts within silica fume and GGBS-rich systems [59-61]. Attention is given to compressive strength evolution and SEM-EDS based microstructural interpretation to reveal hydration product formation and matrix densification [11, 19, 20]. By reducing OPC content by 50% and incorporating industrial byproducts, the binder system presented in this work supports both environmental sustainability and resource efficiency [11-20].

LITERATURE REVIEW

The shift toward low-carbon construction materials has accelerated research into supplementary cementitious materials (SCMs) capable of reducing clinker consumption while maintaining desirable performance characteristics. Industrial byproducts such as silica fume, fly ash, slag, and coal-derived residues have been widely explored for their ability to contribute reactive oxides and participate in pozzolanic or hydraulic reactions within blended binder systems. Studies on coal fly ash and related byproducts demonstrated that coal-origin waste often contains appreciable proportions of silica and alumina, enabling partial reactivity under alkaline conditions and contributing to secondary hydration processes [1]. Investigations into cementation behaviour of coal-derived solid waste confirmed that these materials can influence microstructural densification and binder morphology when properly processed and blended with cementitious matrices [2]. Similar research on rejected coal used as filler materials has shown promising effects on mechanical and durability properties of composite systems, emphasizing the potential for such wastes in construction applications [3]. Fly ash, slag, and coal-related residues have also been examined for their influence on hydration mechanisms. Studies on siliceous fly ash in blended cement pastes identified alterations in hydrate phases, particularly C-S-H and aluminate hydrates resulting from the interaction between fly ash particles and pore solution chemistry [4]. Complementary research on slag- and limestone-blended binders demonstrated that paste composition strongly affects hydration heat release, setting characteristics, and rheological behavior [5]. These findings further highlight the necessity of understanding material compatibility in complex blended systems.

Coal-derived aluminosilicate wastes have been explored beyond traditional cement systems as well, with investigations on geopolymer matrices showing strong mechanical performance and resilient microstructures when coal tailings or gangue materials were activated under alkaline conditions [6]. The reactivity of thermally treated coal gangue has been shown to vary considerably with mineralogical composition, influencing its performance when incorporated into super-sulfated or blended cements [7]. Additional studies on slag-rich binders have demonstrated that binder composition, temperature, and curing regime significantly affect thermo-mechanical behaviour and hydration progression [8]. Research into artificial pozzolanas has further emphasized that temperature and mineral composition govern hydration product formation and microstructural evolution [9]. Thermal analysis of cement pastes has also proven effective in quantifying phase changes associated with hydration and decomposition processes [10], while investigations on limestone slag systems showed that curing temperature significantly influences thermal expansion, phase stability and long-term performance [11].

In parallel, literature highlights the complementary behaviour of silica fume and GGBS in blended binders. Silica fume, with its ultrafine particle size and high amorphous silica content, rapidly consumes calcium hydroxide to form additional C-S-H, accelerating microstructural refinement at early ages [37-40]. GGBS contributes through latent hydraulic reactions activated by alkaline environments, promoting steady strength development and improved durability at later ages. When combined, these materials produce synergistic effects that enhance packing density, reduce permeability, and contribute to stable long-term performance. CWR represents an additional category of SCM suitable for integration into such systems. Although highly variable in composition, many CWR materials contain oxides of silicon, calcium, iron and aluminum that may contribute to filler effects or secondary hydration depending on fineness and chemical characteristics [41-45]. However, due to source-dependent variability, detailed material characterization is essential before incorporation into blended binders [46]. In this study, coal-washery reject material sourced from a major coal beneficiation facility

was utilized after screening and fine processing to evaluate its compatibility within a silica fume and GGBS-rich low-carbon binder [48-49]. Collectively, existing research indicates that combinations of high-reactivity SCMs (such as silica fume) and latent-hydraulic materials (such as GGBS) can be effectively enhanced with suitably characterized coal-derived residues to form sustainable, low-carbon binders.

MATERIALS AND METHODS

This study employed a low-carbon blended binder composed of OPC-53, silica fume, GGBS, and CWR. The CWR used in this investigation was collected from a major coal beneficiation facility and processed as part of the material preparation stage. The complete overview of the material system and the study workflow is illustrated in Figure-1, which presents the binder formulation, material characterization, and primary testing procedures. All materials were prepared before experimentation to ensure uniformity. The coal-washery reject material was oven-dried at 105ºC, pulverized and sieved to pass through a 75 µm sieve to ensure adequate fineness for use as a supplementary component in the binder. Silica fume and GGBS were used in dry form, while the OPC was sourced from a single batch meeting the requirements for 53-grade cement. River sand conforming to Zone II grading and crushed granite coarse aggregates (10 mm and 20 mm fractions) were used as fine and coarse aggregates for concrete preparation.

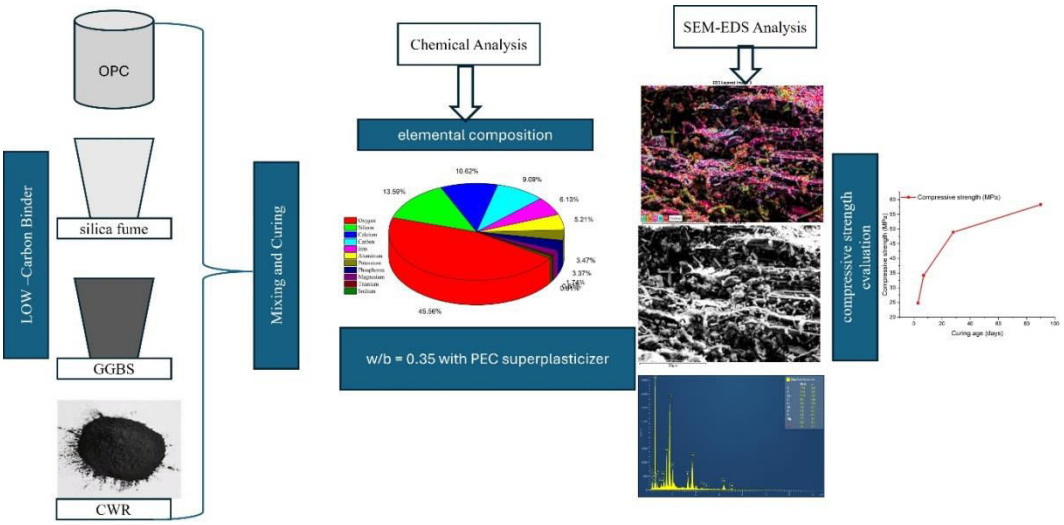

Figure-1. Overall methodological flowchart showing material processing, mixing, curing and analytical procedures.

A polycarboxylate ether-based superplasticizer was incorporated into the mix to maintain desired workability due to the presence of fine mineral additions. The blended binder proportion used in all mixtures consisted of 50% OPC, 20% GGBS, 15% silica fume, and 15% CWR by weight. A constant water-to-binder ratio of 0.35 was adopted for all mixes, with the superplasticizer dosage varied between 0.8-1.2% of the binder weight to obtain consistent fresh properties. The mixing procedure involved initially blending all dry materials for one minute, followed by the gradual addition of water and superplasticizer. Silica fume was added in slurry form to prevent particle agglomeration and ensure homogeneity. After mixing, the fresh concrete was placed in steel moulds and compacted using a table vibrator to eliminate entrapped air. Specimens for compressive strength testing were cast in 150 mm cube moulds, while paste samples were prepared for microstructural characterization. All moulds were demoulded after 24 hours and subsequently cured in potable water at 27 ± 2 ºC until the designated testing ages. Fresh properties such as slump, fresh density and air content were measured immediately after mixing using standard methods. Mechanical testing, including compressive strength evaluation, was performed at 3, 7, 28 and 90 days in accordance with IS: 516 procedures. Microstructural characterization was carried out on hardened paste specimens. Scanning electron microscopy in backscattered electron mode was used to observe hydration morphology and matrix development, while energy-dispersive X-ray spectroscopy was employed to map elemental distributions of O, Si, Ca, Al, Fe, C, K, P, Mg, Ti and Na. Thermogravimetric analysis (TGA/DTG) was used to examine the thermal decomposition behaviour of hydrated phases, and X-ray diffraction was performed to identify crystalline mineral components.

EXPERIMENTAL SETUP AND ANALYSIS

All experimental work was carried out in a controlled laboratory environment using calibrated and standardized equipment to ensure accuracy and repeatability. The fresh properties of the blended binder were assessed immediately after mixing, with workability measured using the slump test as per IS 1199, while fresh density and air content were determined using standard

procedures. For mechanical performance, 150 mm cube specimens were tested for compressive strength at 3, 7, 28 and 90 days in accordance with IS 516, using a 2000 kN digital hydraulic compression testing machine operating under a uniform loading rate. In parallel, representative fragments of hardened paste were prepared for microstructural evaluation by drying, mounting and gold-coating them before imaging. A high-resolution scanning electron microscope operated in backscattered electron mode was used to examine hydration morphology and matrix densification, and energy-dispersive X-ray spectroscopy (EDS) provided elemental distribution maps of key constituents within the hydrated binder. Thermogravimetric analysis (TGA/DTG) was performed under controlled heating to identify mass-loss events corresponding to dehydration, de-hydroxylation and carbonate decomposition, while X-ray diffraction (XRD) was employed to identify crystalline phases formed during hydration. Together, these analytical techniques offered a comprehensive understanding of the chemical activity, phase evolution, and structural development of the low-carbon binder incorporating coal-washery rejects. Details of materials used in the current study are summarized in Table-1.

Table-1. Summary of materials, proportions, and experimental parameters.

Category	Description / Value
Binder Components	OPC (53 grade), Silica Fume (SF), GGBS, Coal-Washery Rejects (CWR)
CWR Source	Major coal beneficiation facility (processed and sieved < 75 μm)
Blended Binder Proportions	OPC 50 %, GGBS 20 %, Silica Fume 15 %, CWR 15 % (by weight)
Water-to-Binder Ratio (w/b)	0.35
Superplasticizer	Polycarboxylate Ether (PCE), 0.8-1.2 % of binder weight
Coarse Aggregate	Crushed granite (10 mm and 20 mm fractions)
Mixing Procedure	Dry mixing (1 min), addition of water + PCE, SF added as slurry
Casting	150 mm cubes (compressive strength), paste samples for SEM–EDS, TGA/DTG, XRD
Curing Condition	Water curing at 27 ± 2 °C
Fresh-State Tests	Slump, fresh density, air content
Mechanical Testing Ages	3, 7, 28, and 90 days
Microstructural Tests	SEM (BSE mode), EDS mapping, TGA/DTG, XRD
Elements Mapped in EDS	O, Si, Ca, Al, Fe, C, K, P, Mg, Ti, Na

RESULTS AND DISCUSSIONS

Fresh Properties of the Blended Binder by Workability

The workability of the blended concrete was assessed using the slump test as per IS 1199. The mix exhibited a slump of 70 mm, indicating medium workability, which is appropriate for laboratory casting and compaction. The presence of finely divided silica fume and processed coal-washery rejects typically reduces free water availability; however, the use of a polycarboxylate ether-based superplasticizer ensured adequate dispersion of binder particles and prevented excessive stiffness. The obtained slump value reflects a cohesive mix without segregation or bleeding, suggesting that the selected w/b ratio of 0.35 and admixture dosage were suitable for maintaining workable fresh concrete.

Fresh Density and Air Content

The fresh density of the concrete was measured immediately after mixing and found to be 2358 kg/m³, which is within the expected range for blended binder systems incorporating silica fume, GGBS and coal-derived mineral additions. The slightly reduced density compared to conventional OPC mixes can be attributed to the lower specific gravity of the supplementary cementitious materials. The air content of the mix, determined using standard procedures, was 2.1 percent, indicating minimal entrapped air and effective compaction during casting. The controlled air content and stable density confirm that the mix possessed uniform fresh-state characteristics and was suitable for achieving consistent hardened properties.

Distribution of Major Elements

Elemental mapping obtained through SEM-EDS, shown in Figures 2-5, illustrates the spatial distribution of key constituents such as oxygen, silicon, calcium,

aluminum, iron, carbon, potassium, phosphorus, magnesium, titanium, and sodium. Silicon and calcium were uniformly distributed throughout the matrix, reflecting the continuous formation of calcium-silicate reaction products. Aluminum and iron were mainly concentrated around partially reacted slag and CWR particles, suggesting their localized role in forming aluminosilicate gel phases. The presence of well-interconnected O, Si, and Ca signals indicates active hydration and secondary reaction pathways typical of SCM-rich blended binders (refer Table-2). The fine and homogeneous dispersion of these elements supports the densification observed in the SEM images.

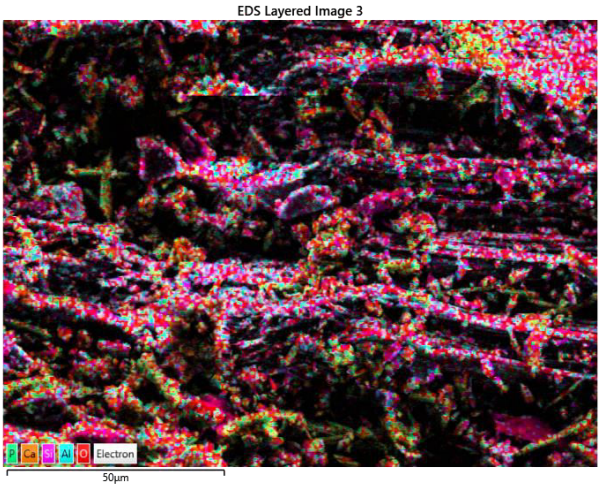

Figure-2. EDS layered image.

Microstructural Characteristics

The Scanning Electron Microscopy (SEM) observations revealed a well-developed hydration structure dominated by C-S-H gel, accompanied by dispersed unhydrated cementitious particles and finely distributed reaction products. The micrographs presented in Figure-5 show a dense and cohesive matrix with reduced capillary voids, which reflect the combined filler effect and pozzolanic reactivity of the incorporated silica fume, GGBS, and processed coal-washery rejects. Plate-like structures characteristic of early C-S-H and partially reacted slag grains embedded within the gel matrix were visible, indicating progressive hydration during curing. The absence of microcracking or coarse porous zones further confirms the stable morphology of the blended binder.

C-S-H Formation and Gel Densification

The SEM analysis revealed extensive formation of C-S-H, appearing as fibrous, foil-like, or layered gel structures within the binder. As shown in Figure-5, the C-S-H gel progressively filled available void spaces, reducing porosity and contributing to matrix compactness. The pozzolanic reaction of silica fume played a major role in consuming calcium hydroxide and generating additional C-S-H, while GGBS contributed through latent hydraulic activation, leading to the formation of more cohesive and tightly bonded gel layers at later curing ages. The densification of gel phases is consistent with the steady strength development observed in the mechanical tests.

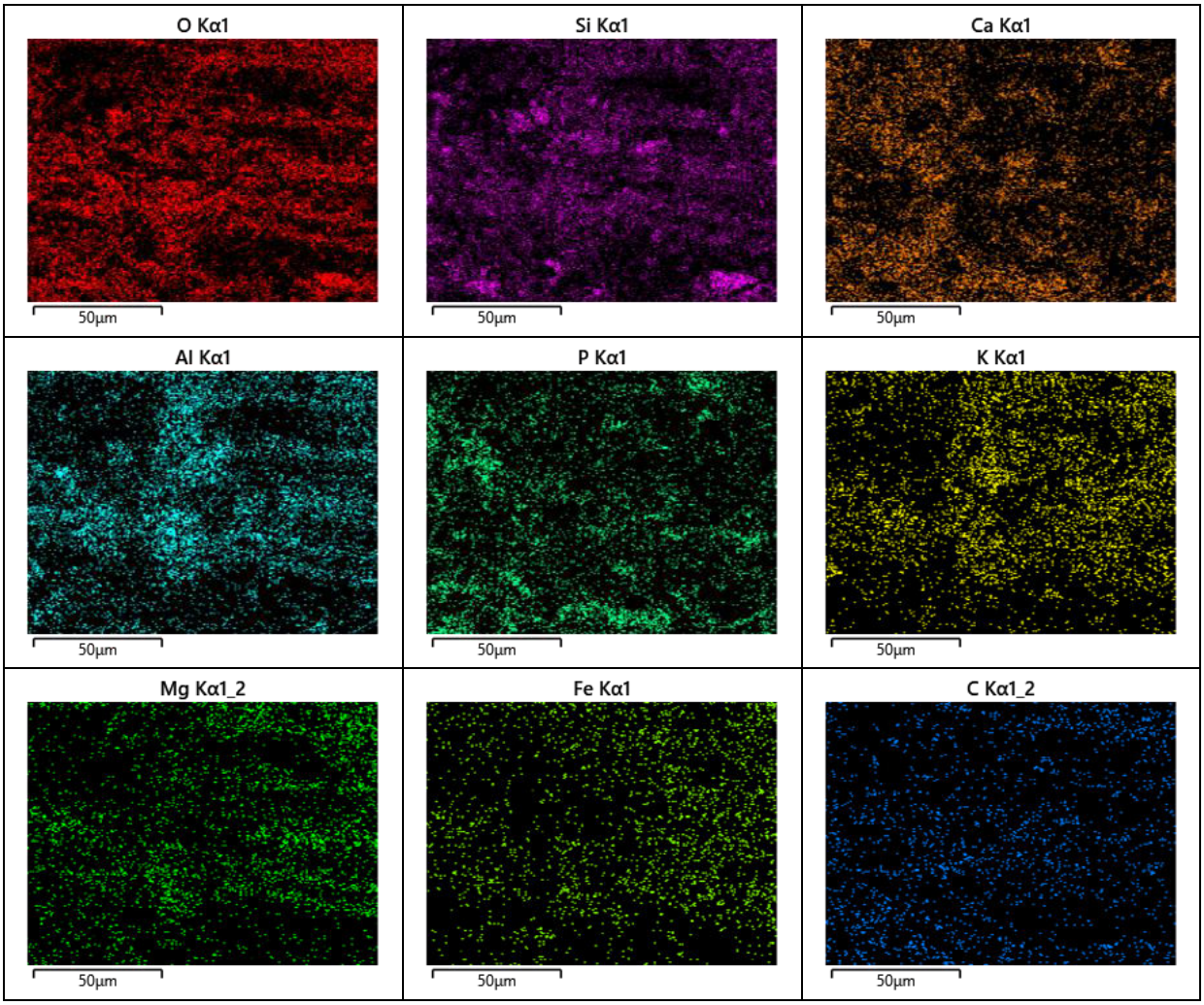

Figure-3. EDS layered images of O, Si, Ca, Al, P, K, Mg, Fe, and C.

Role of Silica Fume, GGBS and CWR in Microstructural Development

The combined influence of silica fume, GGBS, and coal-washery rejects was clearly reflected in the microstructure displayed in Figure-5. Silica fume, due to its ultrafine size and high amorphous silica content, enhanced early pozzolanic activity and contributed to rapid matrix refinement. GGBS participated in long-term hydration, forming additional calcium-aluminosilicate hydrates that improved matrix continuity and strength development. The processed CWR acted both as a microfiller and as a moderate source of reactive oxides, contributing to localized gel formation around its particle surfaces. The combined effect of these materials resulted in a dense, well-hydrated microstructure with reduced pore connectivity. This synergy explains the robust mechanical performance observed across the curing ages.

Thermal Behaviour (TGA/DTG Analysis)

Thermogravimetric analysis (TGA) and derivative thermogravimetry (DTG) were performed to examine the thermal stability and phase decomposition behaviour of the blended binder. The mass-loss trends revealed typical multi-stage thermal events associated with dehydration of gel phases, de-hydroxylation of portlandite and the decomposition of carbonate phases. These transitions provide insights into the extent of hydration, and the contribution of silica fume, GGBS and coal-washery rejects to the formation of stable hydration products.

Dehydration of C-S-H and C-A-H Phases

The initial mass-loss region, occurring between 80°C and 220°C, corresponds to the evaporation of physically bound water and the dehydration of C-S-H and calcium-aluminate-hydrate (C-A-H) gels. The DTG peak observed around 130°C indicates substantial gel formation, consistent with the dense microstructure seen in SEM analysis. The relatively higher bound-water loss is attributed to the pozzolanic reaction of silica fume and the latent hydraulic activation of GGBS, both of which contribute to the generation of secondary C-S-H during early hydration.

Table-2. Elemental composition of coal-washery rejects and qualitative EDS distribution in the hydrated binder.

Element	CWR Composition (wt. %)	Qualitative Distribution in Hydrated Binder (SEM-EDS Observation)
Oxygen	44.6	Uniform distribution throughout hydration products, forming the base of C-S-H and C-A-H phases
Silicon	13.3	Strong presence within C-S-H gel regions and around silica fume–rich areas
Calcium	10.4	Concentrated in OPC hydration zones and slag-activated regions, forming calcium-rich gel layers
Carbon	8.9	Present in carbon-containing residues and dispersed across the matrix in minor amounts
Iron	6	Localized around CWR-origin particles; contributes to iron-modified aluminosilicate hydrates
Aluminium	5.1	Concentrated near partially reacted slag and CWR particles; forms aluminosilicate gels
Potassium	3.4	Evenly distributed in trace quantities across the binder matrix
Phosphorus	3.3	Found around CWR-derived particles; limited involvement in hydration products
Magnesium	1.7	Distributed around slag-related hydration zones; minor role in gel formation
Titanium	0.6	Present in trace amounts; remains mostly inert within the microstructure
Sodium	0.6	Uniformly dispersed in microquantities; influences ionic balance in pore solution

De-Hydroxylation of Portlandite (CH)

The de-hydroxylation of portlandite occurs in the 400-470°C region, with a distinct DTG peak near 445°C. The magnitude of the mass loss in this zone is modest, indicating partial consumption of calcium hydroxide by the pozzolanic reaction of silica fume. The reduced portlandite content reflects efficient conversion of CH into additional C-S-H, confirming the binder's enhanced reactivity and its low-calcium supplementary cementitious characteristics. This trend is consistent with the high proportion of SCMs used in the mix.

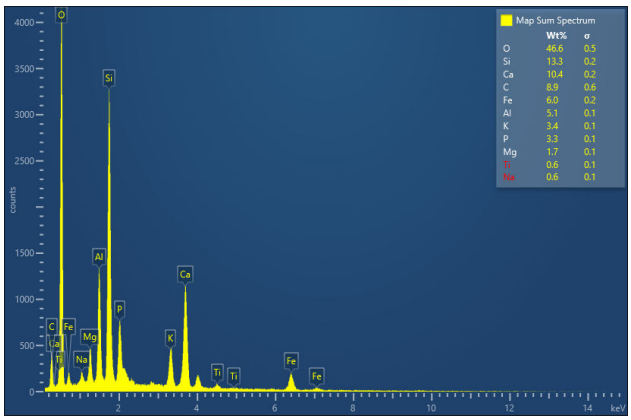

Figure-4. Map of sum spectrum showing the EDS investigation of the mix used in the current study.

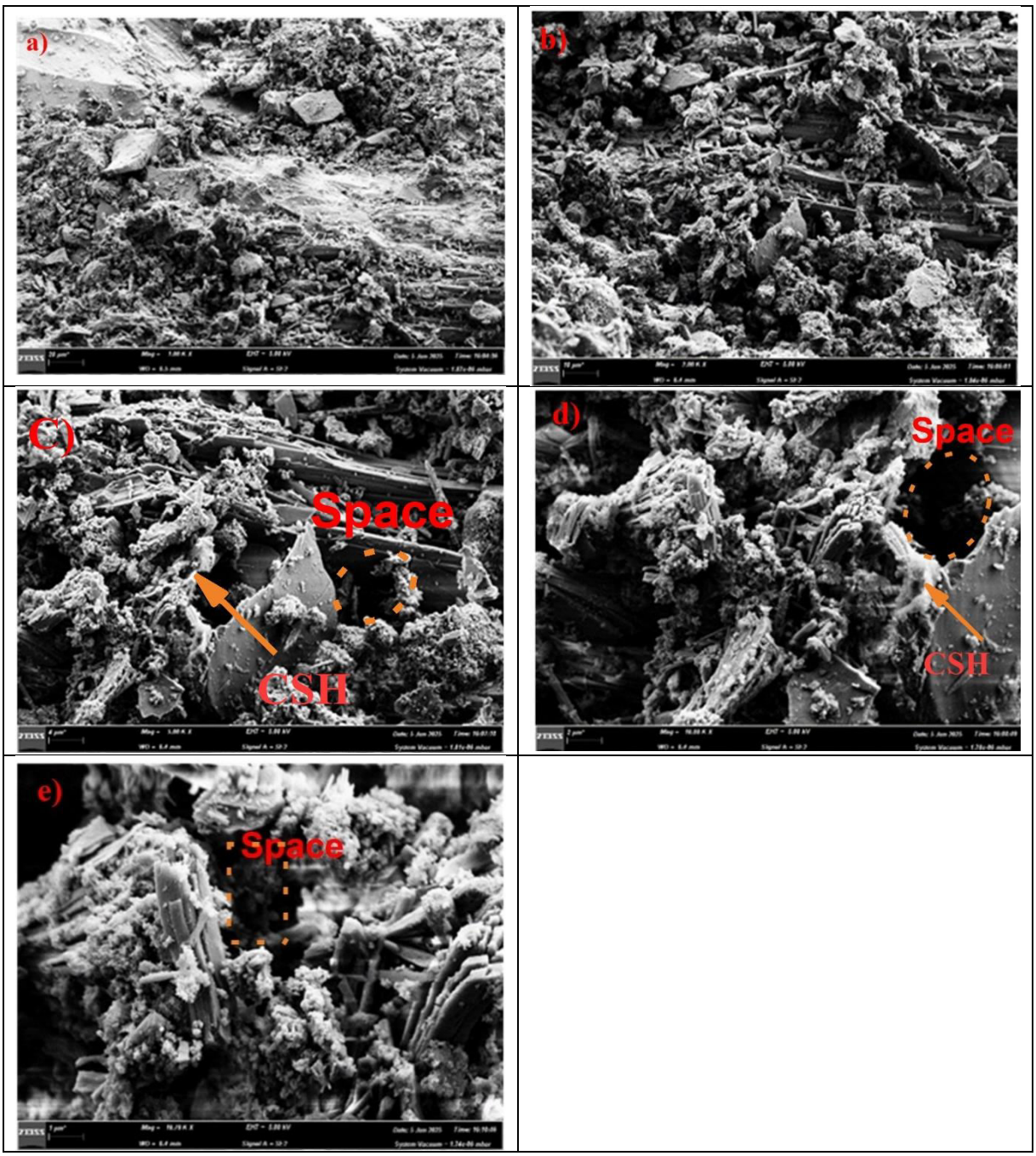

Figure-5. SEM micrograph showing morphology of the concrete mix.

Carbonate Decomposition Events

A broader mass-loss phase between 650°C and 780°C corresponds to the decomposition of calcium carbonate, primarily arising from carbonation of hydration products. The DTG peak centered around 710°C signifies the breakdown of calcite into CaO and CO_2. The presence of carbonate decomposition is typical in blended systems containing slag and fine mineral additions, as their extended hydration period and finer pore structure enhance susceptibility to mild carbonation during curing and handling. However, the magnitude remains within the expected range for SCM-rich binders.

Correlation with Hydration Progress

The combined mass-loss pattern reflects a well-hydrated binder with significant C-S-H development and reduced portlandite reserves, indicating active pozzolanic interaction. The relatively high dehydration-associated mass loss and moderate CH decomposition correlate with the microstructural observations of a dense matrix and well-distributed reaction products. The slag activation and contributions from coal-washery rejects further enhance long-term hydration, as evidenced by the stable carbonate decomposition profile. Overall, the TGA/DTG results (refer Table-3) confirm the progressive hydration pathway

characteristic of systems rich in silica fume, GGBS and mineral additions.

Table-3. Mass-loss events and phase transformations observed during TGA/DTG analysis of the blended cementitious binder.

Temperature Range (°C)	DTG Peak (°C)	Mass Loss (%)	Corresponding Phase Change
80-220	130	4.8	Dehydration of C-S-H and C-A-H gels; physically bound water loss
400-470	445	1.6	Dehydroxylation of portlandite (CH → CaO)
650-780	710	3.2	Decomposition of calcium carbonate ($CaCO_3 \rightarrow CaO + CO_2$)
Total mass loss	--	9.6	Aggregate thermal decomposition

Crystalline Phase Identification (XRD Analysis)

X-ray diffraction (XRD) analysis was conducted to identify the crystalline phases present in the hydrated blended binder and to evaluate the contribution of the supplementary cementitious materials to phase formation. The diffractogram presented in Figure 6 shows a combination of hydration products, unreacted constituents, and secondary phases generated through pozzolanic and hydraulic reactions. The XRD pattern exhibits characteristic peaks associated with calcium-bearing and silicate-based compounds, confirming the formation of a stable hydrated binder matrix. The XRD pattern displays distinct peaks corresponding to calcium-silicate-hydrate (C-S-H) gel, although its largely amorphous nature results in broad humps rather than sharp diffraction peaks. The characteristic amorphous halo centered around 27-34° 2θ indicates the dominance of C-S-H as the primary binding phase. Peaks associated with ettringite (AFt) were identified at approximately 9.0° and 15.9° 2θ, indicating the presence of early-age sulfate hydration products. Minor reflections corresponding to calcium aluminate hydrates were also observed, signifying partial participation of slag and CWR-derived aluminosilicates in hydration. Overall, the hydrated phases confirm an actively reacting binder system supported by the synergistic contributions of OPC, GGBS, and silica fume.

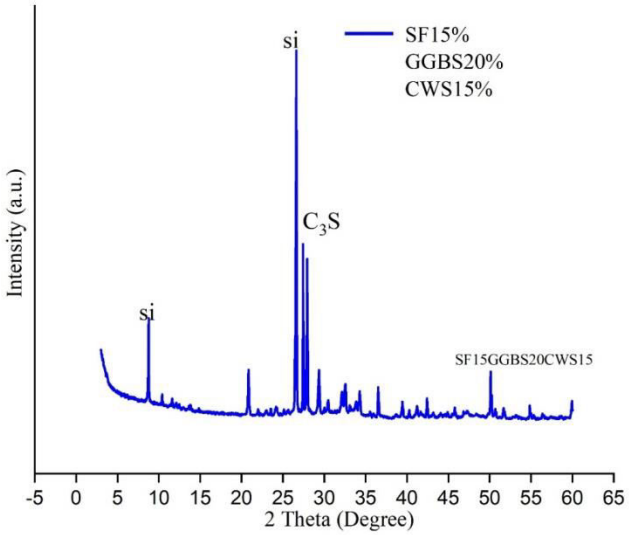

Figure-6. X-ray diffraction (XRD) patterns of the mix id A1.

Unreacted and Partially Reacted Components

Several peaks corresponding to unreacted or partially reacted materials were detected, reflecting the influence of slag, silica fume, and coal-washery components. Quartz peaks at 26.6° 2θ indicate the presence of unreacted silica, attributable to both silica fume and mineral impurities in the CWR. Residual C_3S/C_2S phases were observed at 29.3° and 32.1° 2θ, indicating incompletely hydrated clinker components. Peaks associated with hematite and aluminosilicate phases (from slag and CWR) appeared at 33.2° and 35.6° 2θ, consistent with the elemental distribution reported in the SEM–EDS analysis. These peaks are typical in SCM-rich binders where fine mineral additions remain partially crystalline even after extended hydration.

Influence of SCMs on Crystalline Phase Formation

The blended binder exhibited a reduction in portlandite peak intensity (18.0° 2θ) compared to conventional OPC systems, indicating significant consumption of CH through pozzolanic reactions with silica fume. The inclusion of GGBS contributed to the

formation of additional calcium–aluminosilicate hydrates, reflected by mild increases in low-intensity peaks in the 22–24° 2θ region. The fine mineral fraction of the coal-washery rejects acted as a microfiller and provided alumina, iron and silica sites that influenced secondary phase formation. The combined effect of these SCMs resulted in a more complex crystalline profile with reduced portlandite, increased amorphous content and the presence of stable low-intensity hydration-induced peaks. This aligns with the SEM observations of dense gel formation and with the TGA indication of reduced CH content.

Influence of CWR, SF and GGBS on Mechanical Strength Development

The mechanical performance of the blended binder was strongly influenced by the combined proportions of silica fume (SF), ground granulated blast-furnace slag (GGBS) and coal-washery rejects (CWR). When the CWR content was varied from 5% to 15% at constant SF (15%) and GGBS (20%), a gradual reduction in strength was observed at all curing ages. At 28 days, compressive strength decreased from 49.6 MPa for 5% CWR to 47.9 MPa and 45.2 MPa for 10% and 15% CWR, respectively. The graphical results represent the influence of CWR on the slump in Figures 7-9, and compressive, split-tensile, and flexural strength are shown in Figures 10-12.

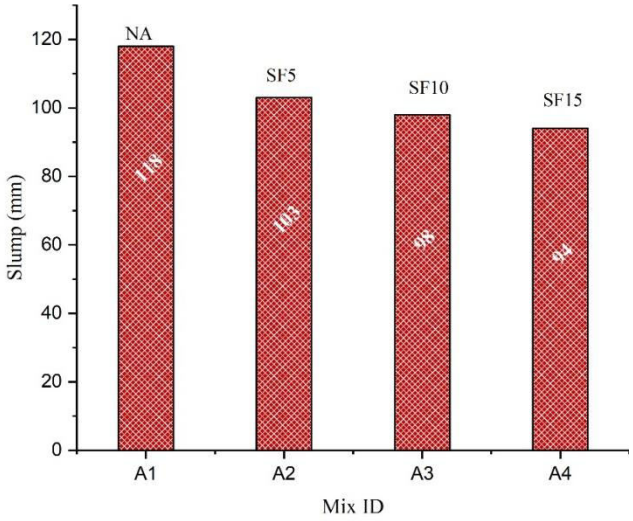

Figure-7. Variation of slump values with respect to differential %s SF (5, 10, and 15).

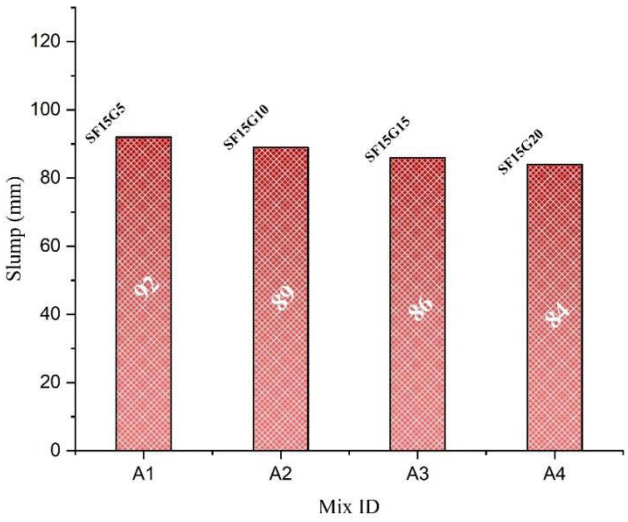

Figure-8. Variation of slump values with respect to SF (15%) and differential %s GGBS.

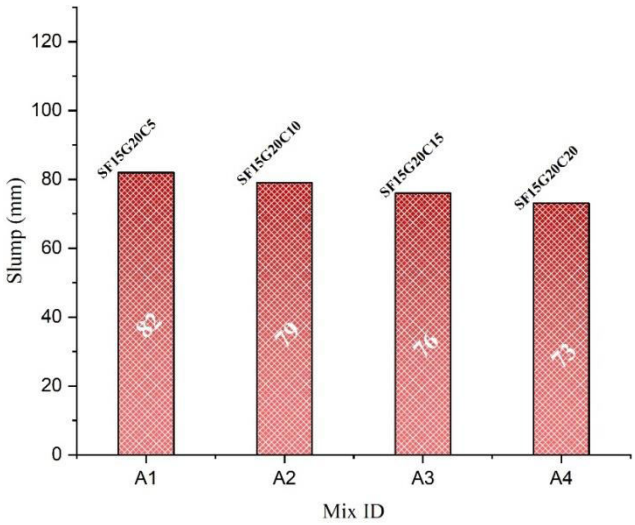

Figure-9. Variation of slump values with respect to SF (15%), GGBS (20%), and differential %s CWR.

A similar decreasing trend was noted in split tensile strength, which reduced from 4.12 MPa to 3.74 MPa, and in flexural strength, which declined from 5.95 MPa to 5.31 MPa as CWR increased from 5% to 15%. This behaviour indicates that while CWR contributes as a microfiller and secondary reactive phase, higher replacement levels reduce the availability of primary cementitious phases, slightly limiting strength development. For mixes with constant CWR content (15%) and varying SF–GGBS combinations (Mixes A1–A4), a progressive enhancement in strength was observed with increasing SCM synergy. At 28 days, compressive strength increased from 46.8 MPa for A1 to 55.1 MPa for A4, representing an improvement of approximately 18%.

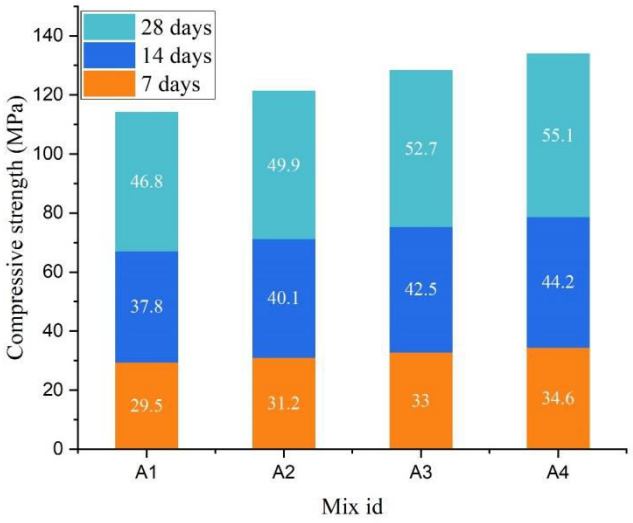

Figure-10. Influence of CWR on the compressive strength of the binder used in the current study.

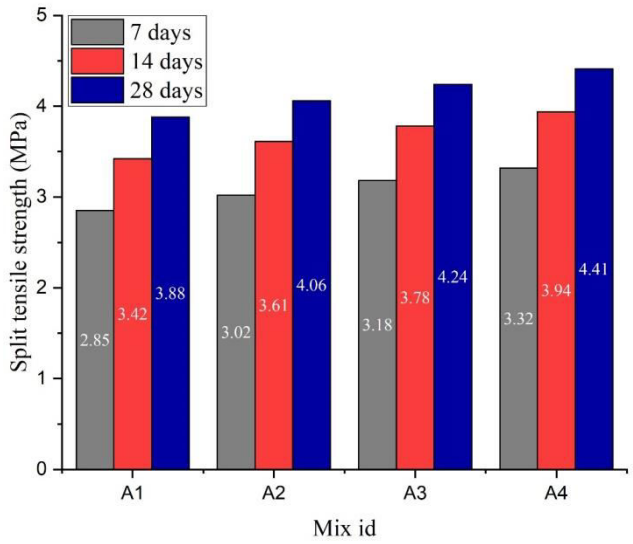

Figure-11. Influence of CWR on the split-tensile strength of the binder used in the current study.

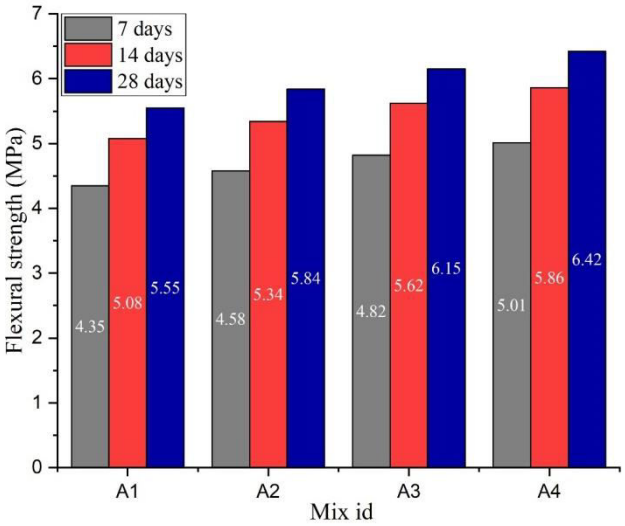

Figure-12. Influence of CWR on the flexural strength of the binder used in the current study.

Correspondingly, split tensile strength increased from 3.88 MPa to 4.41 MPa, and flexural strength improved from 5.55 MPa to 6.42 MPa over the same range. These results demonstrate the beneficial interaction between SF and GGBS, where silica fume enhances early-age pozzolanic activity and matrix densification, while GGBS contributes to sustained hydration and long-term strength development. Overall, the results indicate that CWR can be effectively incorporated up to 15% without severe strength loss when supported by adequate SF and GGBS contents. The combined use of SF and GGBS compensates for the lower reactivity of CWR by promoting secondary gel formation and pore refinement, resulting in balanced mechanical performance across compressive, split tensile, and flexural strength parameters.

ENVIRONMENTAL SIGNIFICANCE

Reduction in OPC Consumption and Carbon Footprint

The replacement of 50 percent of ordinary Portland cement with silica fume, ground granulated blast-furnace slag and coal-washery rejects significantly reduces clinker demand, which is the primary source of CO_2 emissions in cement production. As clinker manufacture involves high-temperature calcination and intensive energy consumption, lowering its proportion in the binder directly decreases process- and fuel-related carbon emissions. The results demonstrate that substantial clinker reduction can be achieved without compromising mechanical performance, thereby supporting low-carbon material strategies and contributing to climate-change mitigation objectives.

Waste Utilization and Resource Efficiency

Coal-washery rejects constitute a major solid waste generated during coal beneficiation, and their

conventional disposal leads to land occupation, environmental degradation, and long-term pollution risks. Incorporating coal-washery rejects at a 15 percent replacement level provides a sustainable pathway for valorizing this waste material by transforming it into a functional component of cementitious binders. The simultaneous use of silica fume and GGBS, both industrial byproducts, further enhances resource efficiency by reducing dependence on virgin raw materials and limiting the extraction of natural limestone and clay. This integrated use of multiple waste streams aligns with circular-economy principles and promotes environmentally responsible material management.

Potential for Environmentally Sustainable Construction Applications

The blended binder exhibits stable hydration behaviour, refined microstructure and consistent strength development, making it suitable for environmentally sustainable concrete applications. Its reduced clinker content and effective utilization of industrial residues support the development of low-carbon construction materials for both structural and non-structural uses. The combined incorporation of silica fume, GGBS and coal-washery rejects offers a practical and scalable approach for producing environmentally responsible binders, particularly in regions with access to coal-processing and steel-industry byproducts. Overall, the developed binder system contributes to sustainable infrastructure development by integrating waste utilization, carbon reduction and long-term performance.

RESULTS AND DISCUSSIONS

The performance of the blended binder incorporating silica fume, GGBS, and coal-washery rejects was evaluated through fresh-state properties, mechanical strength development, microstructural characterization, and thermal and phase analyses. The combined results provide a comprehensive understanding of hydration behaviour and overall material performance. Fresh property evaluation indicated that the mix maintained a medium level of workability, with a slump of 70 mm and stable fresh density, despite the high fineness of silica fume and coal-washery rejects. The measured air content of 2.1 percent confirmed adequate cohesion and compatibility with the selected superplasticizer dosage, enabling uniform casting and consistent hardened performance. Compressive strength exhibited a continuous increase with curing age, reflecting effective hydration of the multi-component binder system. Early-age strength was governed by primary OPC hydration and the rapid pozzolanic reaction of silica fume, while strength gains between 7 and 28 days were enhanced by slag activation and secondary gel formation. Continued strength development up to 90 days indicated sustained hydration activity, which is characteristic of binders rich in supplementary cementitious materials. The progressive strength trend confirms the beneficial combined influence of silica fume, GGBS and coal-washery rejects. Microstructural observations obtained from SEM analysis revealed a dense and homogeneous hydration matrix dominated by well-developed C–S–H gel and finely distributed hydration products. EDS mapping showed uniform distribution of oxygen, silicon, and calcium, indicating extensive gel formation, while aluminum and iron signals reflected the contribution of slag and coal-washery rejects. The absence of large voids or microcracks supported the observed strength performance and indicated good structural integrity. Thermal analysis using TGA/DTG identified distinct mass-loss regions associated with dehydration of C-S-H/C-A-H phases, de-hydroxylation of portlandite, and carbonate decomposition. The moderate portlandite-related mass loss confirmed its partial consumption through pozzolanic reactions, while the carbonate decomposition event indicated stable hydration over time. XRD analysis confirmed the presence of ettringite, residual portlandite, quartz, unreacted clinker phases, and iron-bearing components. The reduced intensity of portlandite peaks combined with a pronounced amorphous hump between 22 and 34° 2θ indicated strong pozzolanic and latent hydraulic activity. Unreacted slag and coal-washery reject particles also contributed through filler and nucleation effects, enhancing particle packing and microstructural refinement. Overall, the hydration mechanism reflects a synergistic interaction among constituents, where OPC provides early reaction products, silica fume accelerates secondary C-S-H formation, GGBS supports long-term C-A-S-H development, and coal-washery rejects act as micro-fillers with localized reactivity. This integrated reaction system results in refined pore structure, enhanced strength, and stable microstructural evolution.

KEY FINDINGS OF THE STUDY

- The blended binder achieved satisfactory workability with a slump of 70 mm, demonstrating good compatibility between supplementary cementitious materials and the superplasticizer.
- Compressive strength increased progressively from 24.8 MPa at 3 days to 58.3 MPa at 90 days, confirming effective hydration and strength contribution from silica fume, GGBS, and coal-washery rejects.
- SEM analysis revealed a dense hydration matrix with well-developed C-S-H gel and reduced pore connectivity.
- EDS mapping confirmed uniform distribution of key elements such as silicon, calcium and aluminum, supporting extensive gel formation.
- TGA/DTG analysis identified dehydration, de-hydroxylation and carbonate decomposition events consistent with stable and progressive hydration.

- XRD results showed reduced portlandite content and increased amorphous gel formation, indicating strong pozzolanic and hydraulic activity.
- Coal-washery rejects contributed through microfiller action and localized reactive sites that enhanced gel development around particle surfaces.
- The binder system exhibited refined pore structure and reduced portlandite levels, supporting its long-term durability potential.
- Replacing 50 percent of OPC significantly reduces clinker-related CO_2 emissions.
- Utilization of coal-washery rejects promotes industrial waste valorization and reduces environmental disposal burdens.
- The binder supports circular-economy principles by converting multiple industrial byproducts into functional construction materials.

CONCLUSIONS

This study investigated a blended binder comprising 50 percent ordinary Portland cement, 20 percent ground granulated blast-furnace slag, 15 percent silica fume and 15 percent coal-washery rejects. The binder exhibited stable fresh-state behaviour, with a slump of 70 mm, fresh density of 2358 kg/m³ and air content of 2.1 percent, indicating good workability and mixture stability. Compressive strength increased from 24.8 MPa at 3 days to 34.2 MPa at 7 days, 48.9 MPa at 28 days and 58.3 MPa at 90 days, demonstrating continuous hydration and effective contribution from supplementary cementitious materials. Microstructural analysis revealed a dense C-S-H-rich matrix with uniformly distributed hydration products. EDS results showed oxygen, silicon, and calcium as dominant elements within reaction zones, confirming extensive gel formation. Thermal analysis indicated mass losses of 4.8 percent due to dehydration of C-S-H/C-A-H phases, 1.6 percent from portlandite dehydroxylation, and 3.2 percent from carbonate decomposition, reflecting stable hydration progression. XRD analysis showed reduced portlandite peaks and a pronounced amorphous hump, confirming enhanced pozzolanic and hydraulic reactions. The integrated hydration behaviour demonstrates that silica fume accelerates secondary C-S-H formation, GGBS supports long-term C-A-S-H development, and coal-washery rejects provide microfiller and localized reactive effects, collectively refining the pore structure and improving strength. From an environmental perspective, replacing 50 percent of OPC significantly lowers clinker demand and associated CO_2 emissions, while incorporating coal-washery rejects promotes waste utilization. Overall, the developed binder exhibits strong technical performance and meaningful environmental benefits, offering a viable low-carbon alternative for sustainable construction applications.

REFERENCES

[1] Agnihotri A. and Ramana P. V. 2022. GGBS-fly ash evaluation in high strength concrete. Materials Today: Proceedings. 50, pp. 2404-2410.

[2] Ahmed A. 2025. Evaluating the performance of low carbon GGBS and metakaolin geopolymer concrete. Journal of Materials and Polymer Science. 5(2): 1-12.

[3] Akintayo B. D., Babatunde O. M., Akintayo D. C. and Olanrewaju O. A. 2025. Transforming industrial waste into low-carbon cement. Recycling. 10(6): 211.

[4] ASTM. 2020. Standard test method for slump of hydraulic-cement concrete. ASTM C143/C143M-20. ASTM International, West Conshohocken.

[5] ASTM. 2023. Standard specification for concrete aggregates. ASTM C33/C33M-18. ASTM International, West Conshohocken.

[6] ASTM. 1990. Standard method of test for compressive strength of concrete specimens. ASTM C39. ASTM International, West Conshohocken.

[7] ASTM. 2017. Standard test method for splitting tensile strength of concrete. ASTM C496/C496M-17. ASTM International, West Conshohocken.

[8] Auxilia Rani A. and Sudha C. 2025. Mechanical and durability performance of fly ash-GGBS geopolymer concrete. Emergent Materials. 8(7): 6039-6056.

[9] Barbhuiya S., Das B. B., Adak D., Kapoor K. and Tabish M. 2025. Low carbon concrete: Advancements and challenges. Discover Concrete and Cement. 1(1): 1-24.

[10] Billong N., Oti J. and Kinuthia J. 2021. Using silica fume-based activator in sustainable geopolymer binder. Construction and Building Materials. 275, p. 122177.

[11] Bradshaw J., Balasubramanian S., Si W., Khan M. and McNally C. 2025. Towards greener 3D printing: A performance evaluation of silica fume-modified low-carbon concrete. Buildings. 15(21): 3919.

[12] Campos Teixeira A. H., Soares Junior P. R. R., Silva T. H., Barreto R. R. and Silva Bezerra A. C. D. 2020. Low-carbon concrete based on binary biomass ash-silica fume binder to produce eco-friendly paving blocks. Materials. 13(7): 1534.

[13] Cheah C. B. and Nurshafarina J. 2019. Influence of silica fume on no-cement mortars. IOP Conference Series: Materials Science and Engineering. 513(1): 012025.

[14] Cheah C. B., Le Ping K. K., Liew J. J., Siddique R. and Tangchirapat W. 2024. Influence of coal bottom ash grading on GGBS mortar. Case Studies in Construction Materials. 21, p. e03739.

[15] Cheruvu R., Rao B. K. and Reddy M. A. K. 2025. Experimental research on sustained concrete with partial substitutions of GGBS, fly ash and silica fume. Journal of Engineering and Technological Sciences. 57(5): 713-734.

[16] Cui W., Dong X., He G., Zhao R. and Liu J. 2025. Environmental implications of red mud solidified with slag and silica fume. Journal of Material Cycles and Waste Management. 27(1): 142-158.

[17] Dhami K. S., Praveenkumar T. R., Giri J., Hassan M. A. and Giri P. 2025. Sustainable concrete mortar using quaternary mix designs. Artificial Intelligence in the Digital Era. pp. 1997-2007.

[18] Duffy G. J., Lanauze R. D. and Kable J. W. 1981. Reducing environmental impact of coal-washing practice. Minerals and the Environment. 3(4): 103-110.

[19] Gao B., Xu L., Tang T., Su K., Chi Y. and Huang L. 2024. Development of low-carbon UHPC with low cement content. Journal of Building Engineering. 94, p. 109907.

[20] Hamad M. A., Nasr M., Shubbar A., Al-Khafaji Z., Al Masoodi Z., Al-Hashimi O., Kot P., Alkhaddar R. and Hashim K. 2021. Production of ultra-high-performance concrete with low energy consumption and carbon footprint using supplementary cementitious materials. Energies. 14(24): 8291.

[21] Hamada H. M., Abed F., Katman H. Y., Humada A. M., Al Jawaher, M. S., Majdi A., Yousif S. T. and Thomas B. S. 2023. Effect of silica fume on sustainable cement concrete. Journal of Materials Research and Technology. 24, pp. 8887-8908.

[22] Hossein H. A., Hamzawy E. M., El-Bassyouni G. T. and Nabawy B. S. 2023. Mechanical properties of synthetic geopolymer binders. Construction and Building Materials. 367, p. 130143.

[23] Hussain S. A., Demrıcı S. and Özbayoglu G. 1993. Identification of clay minerals in coal washery wastes. Applied Clay Science. 7(6): 471-482.

[24] Jena M. S., Priyadarsini A., Tripathy H. K., Mohanty J. K. and Mohanty J. N. 2015. Recovery of clean coal from washery rejects. Transactions of the Indian Institute of Metals. 68(2): 283-289.

[25] Jena S., Panigrahi R. and Sahu P. 2019. Mechanical and durability properties of fly ash geopolymer concrete. Journal of the Institution of Engineers (India) Series A. 100(4): 697-705.

[26] Kumar Poloju, K., Al Ajmi Z., Annadurai S., Hussain A. N. and Rao M. 2025. Experimental study on acid resistance of geopolymer concrete incorporating fly ash and GGBS. Buildings. 15(21): 4012.

[27] Kumar A., Bheel N., Ahmed I., Rizvi S. H., Kumar R. and Jhatial A. A. 2022. Effect of silica fume and fly ash on roller compacted concrete. Environmental Science and Pollution Research. 29(1): 1210-1222.

[28] Kumar A., Kumar P., Gogineni A., Ahmed M. and Chen W. 2025. Evolution of cementitious binders and emerging low-carbon alternatives. Buildings. 15(21): 3811.

[29] Kumar M. H., Saikrishnamacharyulu I., Mohanta N. R., Ashutosh A., Mishra P. and Samantaray S. 2022. Mechanical behaviour of high strength concrete with triple blends. Materials Today: Proceedings. 65, pp. 933-942.

[30] Kumar P. and Singh N. 2024. Performance of recycled aggregate self-compacting concrete. European Journal of Environmental and Civil Engineering. 28(9): 2034-2059.

[31] Kumar P. R., Murthi P. and Poongodi K. 2024. Development of low carbon binder from quaternary blending of cement. AIP Conference Proceedings. 3122(1): 070003.

[32] Kumar R. R., Shalini K., Jawahar J. G., Jagadeesh P. and Rao P. R. M. 2016. Compressive strength of concrete using coal washery rejects. Asian Journal of Civil Engineering. 17(2): 271-276.

[33] Lee J., Lee T., Jeong J. and Jeong J. 2021. Sustainability and performance assessment of binary blended low-carbon concrete using supplementary

cementitious materials. Journal of Cleaner Production. 280, p. 124373.

[34] Liu J., Wu Y., Qu F., Zhao H. and Su Y. 2024. Assessment of CO_2 capture in FA/GGBS-blended cement systems. Buildings. 14(1): 154.

[35] Mahi M. S. H., Jama A. M., Abdi A. A. and Abuu A. A. 2025. Low-carbon concrete development integrating silica fume, glass powder and recycled aggregates. Journal of Engineering Advancements. 6(2): 41-47.

[36] Mohanta S. K., Rout B., Dwari R. K., Reddy P. S. R. and Mishra B. K. 2016. Tribo-electrostatic separation of coal washery rejects. Powder Technology. 294, pp. 292-300.

[37] Mouna Y., Batikha M. and Suryanto B. 2021. Low carbon recycled aggregate concrete: Roles of slag and silica fume. 8th Zero Energy Mass Custom Home International Conference. pp. 1063-1074.

[38] Nafees A., Amin M. N., Khan K., Nazir K., Ali M., Javed, M. F., Aslam, F., Musarat, M. A. and Vatin, N. I., 2021. Modeling mechanical properties of silica fume-based green concrete. Polymers. 14(1): 30.

[39] Nedunuri S. S. S. A., Sertse S. G. and Muhammad S. 2020. Microstructural study of blended Portland cement. Construction and Building Materials. 238, p. 117561.

[40] Nguyen V. M., Tran H. T., Le H. M. and Nguyen V. T. 2025. Experimental optimization of sustainable fine-grained concrete. Frontiers of Structural and Civil Engineering. 19(11): 1935-1949.

[41] Nochaiya T., Wongkeo W. and Chaipanich A. 2010. Utilization of fly ash with silica fume in concrete. Fuel. 89(3): 768-774.

[42] Nukah P. D., Abbey S. J., Booth C. A. and Nounu G. 2022. Optimisation of embodied carbon and compressive strength in low carbon concrete. Materials. 15(23): 8673.

[43] Parcesepe E., De Masi R. F., Lima C., Mauro G. M., Maddaloni G. and Pecce M. R. 2021. Mechanical and thermal properties of alkali-activated concrete. Materials. 14(24): 7717.

[44] Phul A. A., Memon M. J., Shah S. N. R. and Sandhu A. R. 2019. GGBS and fly ash effects on compressive strength. Civil Engineering Journal. 5(4): 913-921.

[45] Ponnudurai V., Rajarathinam R., Muthuvelu K. S., Velmurugan S., Nalajala R. K. and Arumugam L. 2022. Utilization of coal washery rejects for methane production. Chemosphere. 287, p. 132165.

[46] Premkumar R., Hariharan P. and Rajesh S. 2022. Effect of silica fume and recycled aggregates on geopolymer concrete. Materials Today: Proceedings. 60, pp. 211-215.

[47] Rafi D. M., Jayaramireddy B. and Madhava V. 2021. Durability properties of coal washery reject concrete. International Journal of Engineering Development and Research. 9(1): 186-189.

[48] Rathee M., Misra A. and Kolleboyina J. 2023. Mechanical properties of geopolymer mortar with fly ash and GGBS. Materials Today: Proceedings. 93, pp. 377-386.

[49] Rathinam K., Sakthivel S., Vigneshwaran S. P., Vinayagamoorthy M. and Kumar N. 2022. Nano-silica modified geopolymer composite mortar. Materials Today: Proceedings. 62, pp. 535-542.

[50] Reddy G. S. and Ramesh B. 2025. Partial replacements of coarse aggregate using coal wash rejectors. Metallurgical and Materials Engineering. pp. 1422-1423.

[51] Rodríguez J., Frías M. and Tobón J. I. 2021. Eco-efficient cement based on activated coal washing rejects. Construction and Building Materials. 274, p. 122118.

[52] Shubbar A. A., Jafer H., Dulaimi A., Hashim K., Atherton W. and Sadique M. 2018. The development of a low carbon binder produced from the ternary blending of cement, ground granulated blast furnace slag and high calcium fly ash. Construction and Building Materials. 187, pp. 1051-1060.

[53] Shubbar A. A., Sadique M., Shanbara H. K. and Hashim K. 2019. The development of a new low carbon binder for construction as an alternative to cement. Advances in Sustainable Construction Materials and Geotechnical Engineering: Select Proceedings of TRACE 2018, pp. 205-213.

[54] Si W., Hopkins B., Khan M. and McNally C. 2025. Towards sustainable mortar for 3D concrete printing. Buildings. 15(19): 3436.

[55] Singh N., Haque M. M. and Gupta A. 2022. Mechanical performance of geopolymer concrete with coal bottom ash. Materials Today: Proceedings. 65, pp. 1449-1458.

[56] Singh R. P., Vanapalli K. R., Cheela V. R. S., Peddireddy S. R., Sharma H. B. and Mohanty B. 2023. Fly ash-GGBS-silica fume geopolymer concrete. Construction and Building Materials. 378, p. 131168.

[57] Singh S., Ram L. C. and Sarkar A. K. 2013. Mineralogical characteristics of ashes from coal washery rejects. Energy Sources Part A. 35(21): 2072-2085.

[58] Yazıcı H. 2008. Effect of silica fume and high-volume fly ash on self-compacting concrete. Construction and Building Materials. 22(4): 456-462.

[59] Zhao Y., Gao Y., Chen G., Li S., Singh A., Luo X., Liu C., Gao J. and Du H. 2023. Development of low-carbon materials from GGBS and clay brick powder for 3D concrete printing. Construction and Building Materials. 383, p. 131232.

[60] Zhu C., Tan H., Du C., Wang J., Deng X., Zheng Z. and He X. 2023. Enhancement of ultra-fine slag on compressive strength of solid waste-based cementitious materials. Journal of Building Engineering. 63, p. 105475.

[61] Zuaiter M., Khalil A., Elkafrawy M., Hawileh R., Al Hamaydeh M., Ayman A. and Kim T. Y. 2025. Effect of blending GGBS and silica fume on geopolymer concrete. Scientific Reports. 15(1): 9091.